Margot, X.; Escalona-Cornejo, JE.; Bianco, A. (2021). Development of a Novel Numerical Methodology for the Assessment of Insulating Coating Performance in Internal Combustion Engines. SAE International. 1-14. https://doi.org/10.4271/2021-01-0413

2021-01-0413

Development of a novel numerical methodology for the assessment of insulating coating performance in internal combustion engines

X. Margot[1], J. Escalona1, A. Bianco[2]

1. Universitat Politècnica de València. CMT-Motores Térmicos

2. PowerTech Engineering s.r.l.

Abstract

In recent years, the automotive industry has been increasingly committed to developing new solutions for better and more efficient engines. One of them is the use of new insulating materials (thermal conductivity < 0.4 W/m-K, heat capacitance < 500 kJ/m3-K) to coat the engine combustion chamber walls, as well as the exhaust manifold. The main idea when coating the combustion chamber with these materials is to obtain a reduction of the temperature difference (thermal swing) between gas and walls during the engine cycle and minimize heat losses. Experimental measurements of the possible performance improvements are very difficult to obtain, mainly because the techniques available to measure wall temperature are limited. Therefore, simulations are typically used to investigate insulated combustion chambers. Nevertheless, the new generation of insulating coatings is posing challenges to numerical modelling, as layer thickness is very small (~100 μm). Indeed, a detailed modelling would require additional cells refinement for the coating layer and therefore significant increase in computational effort and simulation time. In this regard, a novel strategy to model thin coating layers in the combustion chamber walls is presented in this paper. The approach consists in the definition of a thicker equivalent coating material that reproduces the thermal behavior of the real thin coating. The calculations are performed using a commercial 3D-CFD software for a Diesel engine considering two configurations: conventional metallic piston and coated piston top. Finally, the results are compared to assess the impact of the new generation of insulating coatings on engine performance.

Introduction

Over the past decade environmental regulations in the automotive sector have become more stringent, and the need for more efficient engines has increased considerably. Consequently, during the 2010s, Original Equipment Manufacturers (OEMs) have increased their efforts in the development of new technologies allowing an improvement of Internal Combustion Engines (ICEs) performance. Among the different possibilities, special attention has been given to the application of insulation coatings on the combustion chamber walls, with the aim of reducing fuel consumption, increase engine efficiency and limit any negative effect on pollutant emissions [1].

In this regard, in 2013 researchers from Toyota Corp. research center introduced the “Temperature Swing Insulation Coating (TSWIN)” concept [2]. This consists in coating the engine combustion chamber walls with thin layers (~100 μm) having low heat capacitance and shorter thermal response time, therefore reducing the temperature difference with in-cylinder gases during the engine cycle. The result is an increase in thermal efficiency of the engine without significant drawbacks on other engine performance parameters.

Other authors [3], through numerical simulations, confirmed the hypotheses stated by Toyota that a coating capable of following almost instantaneously the temperature of the combustion gases would lead to 2-4% improvement in thermal efficiency. In particular, both works agree that, in order to obtain the desired thermal swing, the coating material should have 1/32 times the physical properties of zirconia (thermal conductivity of 0.1 W/m-K and heat capacitance of 100 kJ/m^3-K), a material which is typically used in Thermal Barrier Coatings (TBCs).

However, developing a material with such physical properties is not possible yet with the current technology. Even though the investigations on this topic aim at obtaining an optimal coating material, practical advances in TSWIN concept have been carried out by developing coatings characterized by suboptimal properties, in particular concerning the heat capacitance.

In 2016 Toyota presented a material called SiRPA (Silica Reinforced Porous Anodized Aluminum), with a thermal conductivity of 0.67 W/m-K and a heat capacitance of 1300 kJ/m^3-K. This material was used to coat the piston of a turbocharged Diesel engine, specifically the TSWIN 2.4 GD and 2.8 GD engines, reaching a maximum efficiency of 44% [4]. However, in these prototypes the piston bowl

was not coated, therefore the coated portion on the piston surface was limited. In addition, other improvements in the intake and exhaust systems have been included on these engines, hence the 1% reduction in heat losses reported in [4] does not allow to reach a final conclusion on the suitability of SiRPA as a thermal coating.

At the same time, other researchers have put their efforts to find a TSWIN material that allows reducing the heat losses in the combustion chamber. In this sense, the United States Department of Energy (U.S. Dept of Energy) and the Advanced Research Projects Agency – Energy (ARPA-E) have opened the way for a new generation of TBCs with increased benefits [5]. The coatings developed under this project showed significant improvements in physical properties compared to Toyota's SiRPA, such as a thermal conductivity lower than 0.40 W /m-K and heat capacitances lower than 500 kJ/m^3-K. This work was carried out in cooperation with the University of Wisconsin-Madison and they used binders mixed with aluminosilicate, metals and oxide powders to decrease the conductivity, density and specific heat capacity of the coating material. This technology was evaluated with different coated configurations on a Spark Ignition (SI) engine and the results highlighted the polysilazane coatings as the best candidate to serve as an insulating material in ICEs. Furthermore, a reduction of 4% in heat losses was achieved, as well as an improvement in thermal efficiency of the engine of about 1.1-1.3%. In addition, researchers were able to prevent the engine from entering in knocking regime.

Despite the possible improvements, validating these claims through traditional experimental techniques is quite complicated. In fact, due to the characteristics of the coating, it is difficult to place thermocouples on the surfaces of the combustion chamber walls. In addition, thermocouples' response time does not allow investigating the combustion chamber surfaces temperature evolution with crank-angle resolution. Hence it is strictly necessary to use other techniques to measure the temperature of the solid surfaces. In order to solve this problem, Fukui et al. [6] presented a method to measure the instantaneous temperature in the coated walls through optical techniques. The methodology proposed, however, is affected by some uncertainties concerning the temperature swing measured on the surface of the aluminum piston. The resulting piston temperature, for example, is considerably higher than that found by several other authors through numerical simulations and experimental tests performed with thermocouples [7,8], consequently the reliability of the different experimental techniques is still unclear. In view of the above-mentioned limits, there is not nowadays any specific experimental technique that can provide sufficient details concerning combustion chamber coating thermal behavior during engine cycles.

The numerical models appear as a natural alternative to study the heat losses in ICEs. In particular, 3D-CFD calculations have the potential to yield accurate information about the heat transfer between in-cylinder gases and combustion chamber walls. However, simplifications are typically made during the analysis of in-cylinder processes, among which the most relevant for heat transfer analyses is the assumption of constant combustion chamber wall temperatures throughout the full cycle. This assumption can affect the combustion simulation and lead to inaccuracies, especially if a TSWIN coating is present. To overcome this limit, Conjugate Heat Transfer (CHT) in-cylinder simulations are required, which are recognized as one of the most suitable methods to study the heat transfer in ICEs [9]. In CHT calculations the fluid and solid domain (e.g. piston) are both considered and the heat transfer between the two regions is accounted for during the whole simulation. This approach allows the study of spatial and temporal temperature distribution on any solid surface, plus the calculation of local heat transfer coefficient between the solid and the fluid and its temporal evolution.

Currently, in literature there are many studies concerning the application of insulation coatings in ICEs. However only few of them deal with 3D-CFD studies of ICEs with coated combustion chamber walls [10-12]. Among them, to the authors' knowledge there are no CHT studies concerning the new generation of TSWIN insulating coatings material. This is probably due to difficulties in the calculation of gas-solid heat transfer when very thin coating layers (~100 μm) are present, which lead to significant computational costs [13,14]. Additionally, the lack of available experimental data constitutes a clear limit to numerical simulations, as they cannot be validated against reliable measurements. It is worth highlighting, however, that numerical simulations are therefore the only available tool that can provide all the details concerning the coating thermal behavior and its effects on in-cylinder processes, albeit without explicit validation of the results.

In this framework, the main objective of the work described in this paper is to study the heat transfer through the thin coated combustion chamber walls of an ICE and assess its effect on performance. The study was performed on a Diesel engine at high speed – medium load operating point, whose characteristics are briefly summarized in the engine geometry section. Two engine configurations were studied: conventional metal piston and coated piston top (piston bowl was not coated). A methodology to define the properties of an equivalent thick material was employed to overcome the difficulties concerning the simulation of a thin coating layer and is summarized in the methodology section. The 3D-CFD numerical setup is then described. Finally, results of the two piston configurations are compared in order to determine the impact of the coating layer on engine performance.

Geometry and engine specifications

The engine selected for the study was a 1.6L, four-cylinder, turbo-charged Diesel engine equipped with a common rail injection system and it was characterized experimentally in a test bench at CMT facilities. The tests were performed with a 6-nozzle injector with holes diameter of 124 μm and a spray angle of 150º. In-cylinder pressure signals were measured in the four cylinders with piezoelectric transducers, sampled using a dedicated acquisition system and recorded during 50 consecutive engine cycles [15,16].

Table 1. Main engine features and operation condition.

Number of cylinders [-]	4-in line
Bore – stroke [mm]	75.0 – 88.3
Connecting Rod [mm]	137.1
Compression ratio [-]	18:1
Number of valves [-]	2 intake and 2 exhaust
Torque [Nm]	23.7
Engine Speed [rpm]	3500
Air fuel ratio [-]	1
Start of injection [CAD aTDC]	-11
Number of injections [-]	1
Injection pressure [MPa]	97

A high speed - medium load operating point was selected for the analysis, in order to limit the simulation time, which would be longer for low-speed operations [17-19]. The details about the main engine features and the operating point are listed in Table 1.

Methodology

Insulating coating layers in recent engine applications are characterized by a very small thickness (~100 µm) which, from the computational point of view, leads to a significant increase of the modelling effort and computing time in 3D CHT simulations, due to the necessity of extremely refined grids. In this regard, a methodology to numerically assess the heat losses through coated combustion chamber walls with reduced computational effort has been developed [20], which is briefly summarized in Figs. 1 and 2 and described in the following sections. The concept is to replace the very thin coating layer (thickness e) and the base aluminum substrate in contact with it (thickness L) by an equivalent coating layer of total thickness (L+e) allowing reasonable mesh sizes, as shown in Fig. 1. From the thermal perspective the thick coating layer can be considered equivalent to the real coating aluminum substrate if its temperature evolution along the engine cycle matches that of the real piston layers when subject to the same boundary conditions.

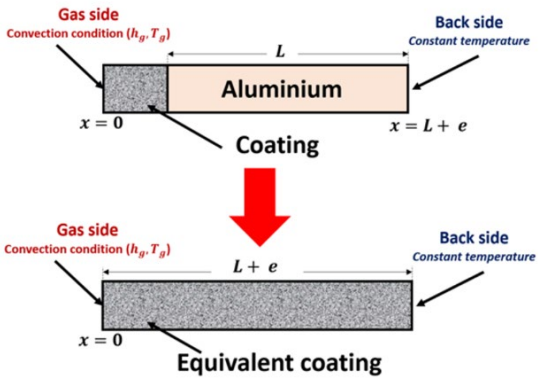

Figure 1. Schematics of thin coating layer with adjacent aluminum and equivalent thick coating layer dimensions.

As indicated in the schematic representation of Fig. 1 the thin coating layer which is in contact with the aluminum substrate is exposed to the in-cylinder gases. On this boundary, the near-wall heat transfer coefficient h_g and the average gas temperature T_g are imposed. The back side of the piston substrate is exposed to a constant temperature boundary (430 K), since the internal piston temperature can be ascribed as constant during the engine cycle, provided that the aluminum thickness L is sufficiently large (high heat capacity of the metallic materials). The equivalent coating layer is also shown in Fig. 1 (bottom) and is exposed to the same boundary conditions. For modelling purposes, the thickness L can be conveniently set to values much higher than the real coating layer thickness e, thus allowing the description of the equivalent coating layer with coarser meshes.

In the proposed approach a 1D heat transfer model was used in combination with a multi-factorial DoE and a multiple regression analysis to define the thermodynamic properties (conductivity and heat capacitance) of an insulating layer equivalent to the real thin coating and adjacent metallic substrates in terms of heat fluxes and temperature evolution. An iterative strategy was adopted for identifying the physical properties of the equivalent thick coating layer material, which is further described in the following section.

Equivalent coating definition

In the simulations of the coated piston configuration the material proposed by Andrie et al. [5] was used as a reference. The authors reported improvements on the performance of a gasoline engine by applying the selected insulating material on the combustion chamber walls. The properties of this material are:

- Thermal conductivity: 0.35 W/m-K
- Heat capacitance: 400 kJ/ m^3-K
- Thickness e: 100 µm

For the aluminum layer, the following properties were considered:

- Thermal conductivity: 144 W/m-K
- Heat capacitance: 2316 kJ/ m3-K
- Thickness L: 1.9 mm

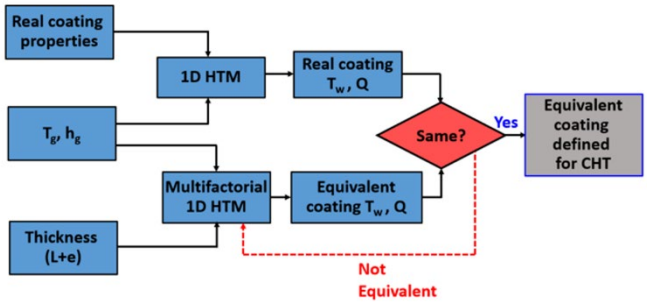

Figure 2. Iterative numerical procedure adopted for the identification of an equivalent coating layer.

As summarized in Fig. 2, starting from material properties and in-cylinder conditions (gas temperature T_g, gas-piston heat transfer coefficients h_g) a 1D heat transfer model (1D-HTM) [21] was used to determine the thermal behavior of the coating material (gas side wall temperature T_w, heat transfer Q). In this lumped model, which is only briefly summarized in the following, the system was modeled as a thermal network where the heat transfer for each node can be described with equation 1.

$$[K][T^t] - [C][T^t] = [T^{bc}] - [C][T^{t-\Delta t}] \quad (1)$$

where:

$[T^t]$: is a temperature vector (unknown)
$[K]$: is the conductance matrix
$[C]$: is the capacitance matrix
$[T^{bc}]$: is the temperature vector of boundary conditions
$[T^{t-\Delta t}]$: is a temperature vector (previous step)

The transient in-cylinder gas temperature and heat transfer coefficient shown in Fig. 3 were used as input parameters in the model. These values were calculated with a combustion diagnosis tool [16] using the experimental data available for the Diesel engine under study at a low speed – high load operating point, Experimental working conditions were considered compatible with the engine working point

under study in terms of heat rejection.. For the discretization of the coating and adjacent aluminum layer 500 nodes were used for the 1D mesh, 400 nodes of which were placed in the thin coating. As discussed in [20], the number of nodes used to describe the equivalent thick coating layer in the 1D-HTM should match the one used in 3D-CFD-CHT simulations, since there is a tight coupling between the number of nodes and the physical properties of the equivalent coating layer material. In particular, if the number of nodes used to describe the thick coating layer changes, then also the properties of the equivalent coating material will change ([20]). In the present study 4 nodes were used to describe the 2 mm thick equivalent coating layer, consistenly with 3D-CFD-CHT mesh settings introduced afterwards.

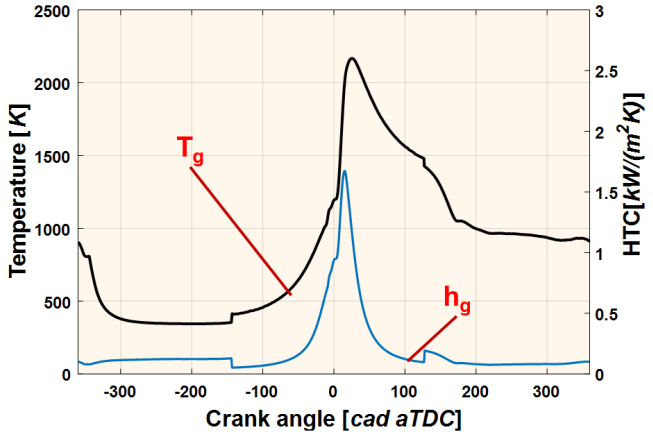

Figure 3. In-cylinder gas temperature (black) and gas-wall heat transfer coefficient (blue) used as boundary conditions in the 1D-HTM.

The 1D-HTM yields as outputs the temporal evolution of the wall temperature (T_w) and heat flux (Q) of the thin coating and aluminum layers set, which were considered as references for the definition of a thick coating substrate.

A multifactorial DoE test with the 1D-HTM was then performed for selected physical properties (thermal conductivity and heat capacitance) of the equivalent thick layer material. In this sense, the inputs range for the DoE were:

- Thermal conductivity: 5 - 10 W / m-k
- Heat Capacitance: 0 - 30 kJ / m^3-K

Fig. 4 shows the temporal evolutions of the wall surface temperature and heat flux for the real coating and the candidate equivalent coating materials obtained with the multifactorial DoE.

Finally, a multiple regression analysis was used to statistically identify the properties of the best equivalent material. Positive (q_+) and negative (q_-) heat transfers between coatings and in-cylinder gases during the engine cycle, defined in equations (2) and (3) respectively, were considered as selection criteria.

$$q_+ = \int_{t1}^{t2} \dot{Q}_{gas \to wall} dt \quad (2)$$

$$q_- = \int_{t1}^{t2} \dot{Q}_{wall \to gas} dt \quad (3)$$

The heat transfers calculated considering the real coating and the aluminum layers were considered as references. Then, the differences between the heat transferred by the candidate equivalent coatings and the references were defined as:

$$q_{+/-}^{error} = \left(1 - \frac{q_{+/-}^{equivalent}}{q_{+/-}^{real\ coating}}\right).100 \quad (4)$$

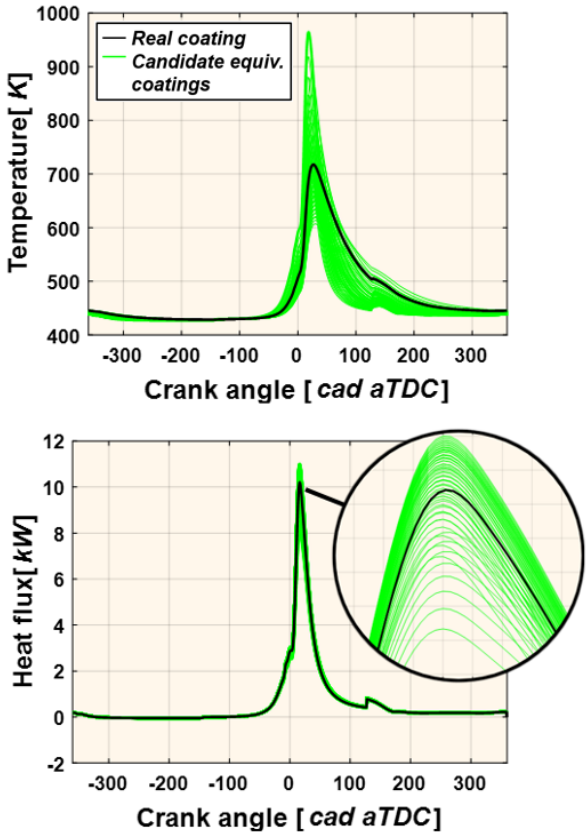

Figure 4. Temporal evolution of gas exposed surface temperature (top) and heat flux (bottom) for real thin coating with aluminum substrate (black) and candidate equivalent coating materials (green), as calculated with the 1D-HTM.

Fig. 5 shows the results of the multiple regression analysis: the tradeoff between heat transfers is represented for all the investigated equivalent coating materials. The best equivalent coating material properties were selected as those minimizing heat transfers differences (starred point). Clearly, small deviations in the properties of the equivalent material can increase the error significantly. The selected equivalent material has a thermal capacitance of 17.6 kJ/m^3-K and a thermal conductivity of 5.2 W/m-K. It is worth highlighting that these properties do not need to represent an existing material. Indeed, they are instead used only to reproduce the thermal response of the thin coating and the aluminum substrates by means of a thick equivalent layer, during the engine cycle.

Fig. 6 shows a comparison of the temperature and heat flux profiles characterizing the original thin coating with adjacent aluminum layers and the equivalent thick layer during the engine cycle. Both traces, heat flux and transient temperature are almost over-imposed throughout the cycle, with maximum errors of 0.7 %, -0.2%, -0.2% in

negative, positive, and mean heat transfers respectively, and 3.9% in temperature.

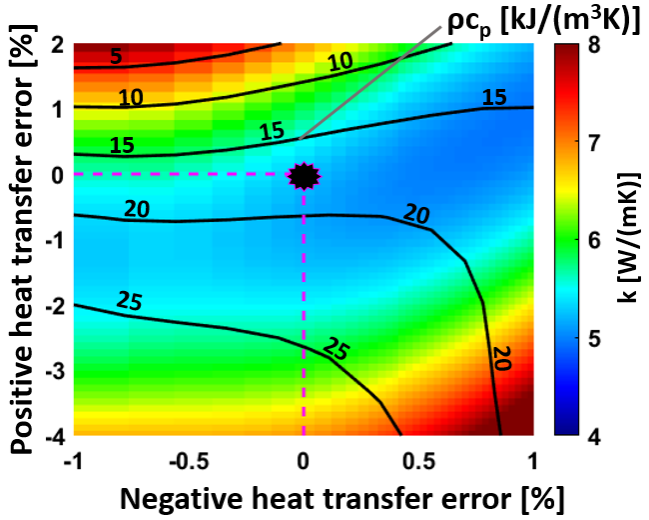

Figure 5. Selection of material physical properties for the equivalent coating layer via a multiple regression analysis.

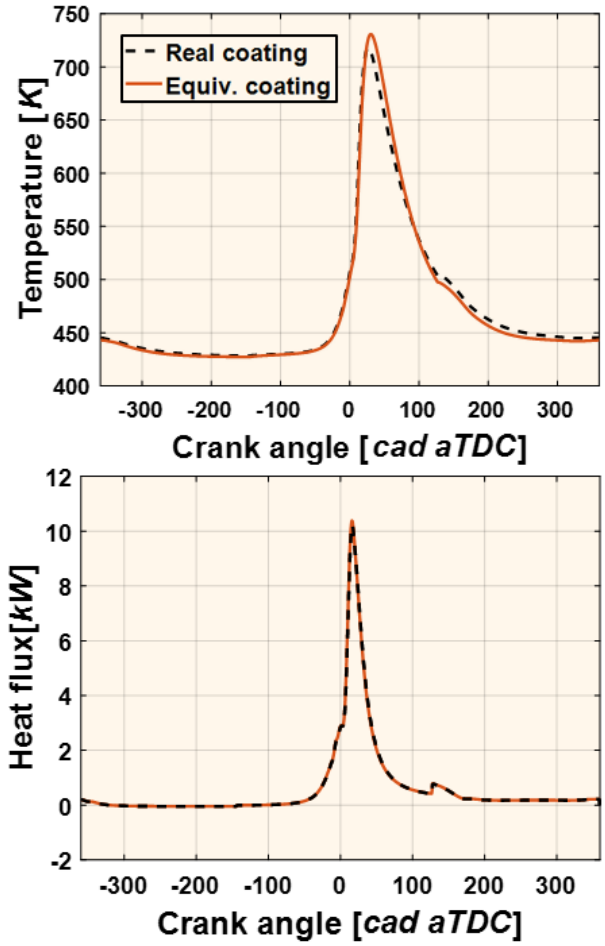

Figure 6. Comparison of the gas exposed surface temperature evolution (top) and heat flux evolution (bottom) for the real coating (black) and the selected equivalent coating material (orange) calculated with the 1D-HTM.

Finally, the selected physical properties of the equivalent coating layer material, i.e., the calculated thermal capacitance and thermal conductivity were used in 3D-CFD-CHT simulations. The equivalent coating material density was set to 1000 kg/m^3 and the specific heat capacity was set to 17.6 kJ/kg K, to match the calculated thermal capacitance, as the latter is the only relevant quantity affecting heat transfer analyses. Variations of material physical properties with temperature were neglected in the study.

Numerical setup

In this work, 3D-CFD simulations were performed on a domain representing the combustion chamber, intake and exhaust ports as shown in Fig. 7. In addition, the solid piston was also included for the CHT calculations.

The commercial 3D-CFD code CONVERGE [22] was used. Multicycle simulations allowed reaching steady-state cycle-averaged thermal conditions in the solid and a speed-up strategy involving the so-called super-cycling model was adopted. The approximate calculation time was 3 days/cycle using 32 cores. A brief description of the mesh settings, models and boundary conditions is presented in the following sections.

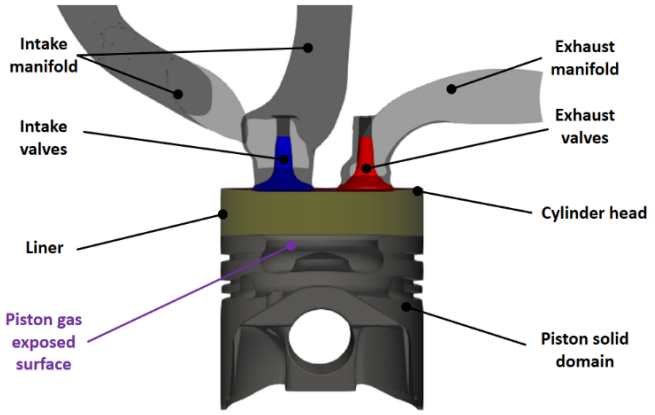

Figure 7. Computational domain used for 3D-CFD CHT calculations. Gas exposed surfaces of the piston represent the fluid/solid interface.

Mesh generation

The mesh was generated automatically by CONVERGE at runtime using a modified cut-cell Cartesian grid generation method, in which the user can customize the base grid size. Usually, in CFD calculations a base grid size is adopted with uniform dimensions in the three spatial directions, and according to the previous work of Gomez-Soriano [23] a base cell size of 3 mm is sufficient to model the combustion process in the Diesel engine under study. In order to limit the cell count and allow the description of the thick coating layer with an integer number of cells, a non-uniform base grid size was adopted in the simulations. More in detail, the base grid size was set to 3 mm in directions perpendicular to the cylinder axis, while it was set to 2 mm along the cylinder axis. These settings allowed the modelling of the equivalent coating layer with exactly 4 nodes,

thanks to a limited local mesh refinement, and assured a sufficient resolution of the fluid zone according to previous studies.

The computational grid was further refined in specific regions where high gradients of physical quantities were expected or observed. For spray modeling, an injector shaped refinement was used at the injector location, leading to local cell sizes of 0.375/0.25 mm. Furthermore, the Adaptive Mesh Refinement (AMR) approach was adopted to refine the mesh in zones of the combustion chamber where the velocity and temperature gradients were the highest. In this context, the grid was automatically refined in order to limit the estimated error on the velocity and temperature fields to a maximum of 1 m/s and 2.5 K respectively, using a minimum grid size equal to 0.75/0.5 mm.

To optimize the CHT calculations and limit cell count, a strategy aiming at achieving the desired value of near-wall y+ using the AMR approach was employed. The method consists in defining the maximum and minimum y+ target on selected boundaries and allow the refinement of cells by the AMR algorithm only where and when needed, thus reducing the computational weight of the simulation compared to a fixed embedding strategy. Although the numerical resolution of the thermal and kinetic boundary layers would be the preferred choice in CHT simulations, this strategy is computationally expensive especially when multiple engine cycles are to be simulated. The wall-function approach was therefore adopted in the study, with standard wall functions, and the y+ was targeted to be between 30 and 300 following the available best practices [24,25]. In particular, a permanent AMR was adopted on the fluid side of the combustion chamber walls (piston, liner and cylinder head) to achieve the target y+, with a minimum cell size set to 0.75/0.5 mm. This setting is consistent with the local grid refinement adopted for the coating layer, where cell size was set to 0.75/0.5 mm which assured that the grid on the solid side of the fluid-solid interface was equal or finer than the one on the fluid side [22]. These settings effectively limited the interpolation error between data on the fluid and the solid side of the fluid-solid interface.

An example of the resulting computational mesh employed for the calculation at a specific crank angle is shown in Fig. 8.

Models and boundary conditions

Fuel injection was modelled using settings from previous studies [23]. As far as the liquid fuel is concerned, the DIESEL2 fuel surrogate [22] was adopted, which has been employed by several authors for spray modeling in CI engines [26]. In addition, liquid film formation due to spray-wall interactions was included in the analysis and was described with the O'Rourke film model [27].

The combustion process was simulated using the SAGE combustion model [28]. The RNG (renormalization group) k-ε model was used for turbulence combined with the O'Rourke and Amsden heat transfer wall model [27,29], the selection being based on previous studies carried out in ICEs [18].

In order to optimize the calculation time, the time step-control strategy adopted in [30] was employed, which allowed the relaxation of the Courant Friedrichs Lewy (CFL) constraint during specific stages of the engine cycle.

Additional boundary conditions such as fuel mass, injection rate and intake/exhaust ports pressure and temperature were imposed according to the experimental data.

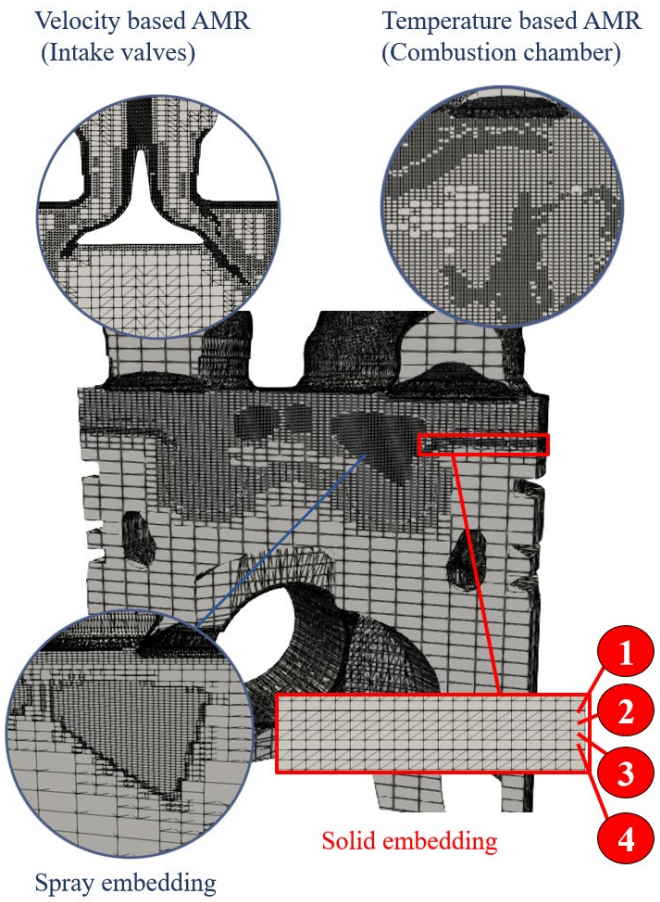

Figure 8. Mesh excerpt of the CI engine at a specific crank angle. Coating insulating layer is meshed with 4 nodes (labelled as 1-2-3-4).

Liner and cylinder head were modelled as isothermal walls and temperature levels were set consistently with experimental data acquired by means of thermocouples (389 K for the liner and 406 K for the cylinder head). The piston wall temperature was a result of the CHT calculation, for which specific boundary conditions were imposed in the solid domain, following the same approach employed in previous works [20]. The piston surface exposed to combustion gases was divided in two boundaries in order to separate the coated piston top from the bowl. The rest of the piston surface which is not directly exposed to combustion gases was divided in several boundaries, as shown in Fig. 9.

In general, it is difficult to prescribe boundary conditions for solid regions in Diesel engines due to the presence of the cooling gallery inside the piston. To overcome this difficulty, the division proposed by Gonera et al. [31] was adopted. In order to simplify the problem, the transient effects of oscillating fluid velocities in the oil gallery and thermal dilatation of solid walls were neglected in the analyses. For the internal side of the skirt and the oil gallery the correlations proposed by Lu et al. [32] and French [33] were used, respectively.

Other boundary conditions on piston surfaces were estimated with an equivalent thermal circuit methodology as proposed by Esfahanian et al [34].

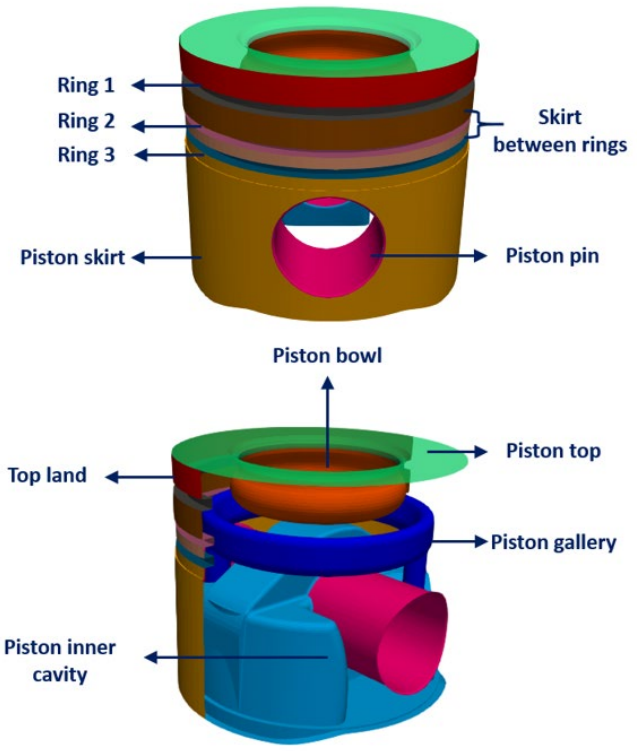

Figure 9. Piston boundary conditions considered in the CHT solid domain. Piston top and piston bowl represent the fluid/solid interface in the calculations.

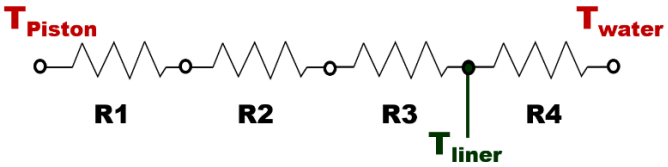

Figure 10. Scheme of the thermal circuit adopted for the calculation of boundary conditions at the piston surfaces (Esfahanian et al [34]).

Table 2. Boundary conditions for the engine piston surfaces.

Boundary	Temperature [K]	HTC [W/m^2-K]
Top land	451	91
Piston ring 1	421	1108
Piston ring 2	381	828
Piston ring 3	371	984
Piston skirt	363	115
Skirt between rings	363	115
Piston inner cavity	363	612.5
Piston pin	363	612.5
Piston gallery	374	6384

Fig. 10 shows a scheme of the thermal circuit used for the definition of piston boundary conditions, with R_i the thermal resistances due to the various elements interposed between the piston and the water jacket coolant (e.g., piston rings, oil film, liner, etc.). Table 2 shows the resulting boundary conditions calculated with the thermal circuit approach.

Lastly, one of the main problems in CHT simulations is the diversity of timescales which can differ by orders of magnitude between fluid and solid. Hence, the calculation of the steady-state thermal behavior of the system requires long simulations. In order to limit the simulation time and reduce the computational effort, the super-cycling [22] model was adopted in this study, which is an acceleration method that solves time-dependent CHT problems as steady-state in solids. When super-cycling is enabled, heat transfer between fluid and solid regions is solved for a user-defined time interval, as in standard CHT simulations. During this period Heat Transfer Coefficients (HTCs) and Near Wall Temperatures (NWTs) are stored for each cell at the fluid/solid interfaces. When the user-defined time interval is reached the solver freezes the fluid region and time-averaged HTCs and NWTs are converted to boundary conditions for the solid region. Heat transfer inside the solid is calculated with a steady state solver until the solid temperature field reaches convergence, completing the Super-Cycle stage. At this point the solid region temperature field is updated, the fluid region is unfrozen and the standard CHT simulation is run for another Super-Cycle stage. The described strategy allows the simulation of thermal dynamics involving fluids and solids in a reduced simulation timeframe, thanks to the superposition of steady-state thermal conditions for the solid region. For a cyclic system such as an ICE, the time-averaged data should represent an entire engine cycle, therefore in the present work 12 super-cycling stages with 60 CAD duration were adopted. After the first engine cycle is completed, the software executes the first Super-Cycle stage. During successive cycles the Super-Cycle stage is repeated every 60 CAD considering HTCs and NWTs stored during the previous 720 CAD. With the described strategy the simulation of four full engine cycles was found to be sufficient to achieve a steady-state cycle-averaged piston thermal field for both the coated and the conventional piston configurations.

One additional engine cycle was finally simulated without the Super-Cycling model, in order to investigate the transient thermal behavior of the solid piston once a constant cycle-averaged temperature was reached. The simulation of a single cycle was found to be sufficient to describe the transient evolution of solid temperatures, as the cycle-to-cycle temperature variation observed at the end of the last simulated cycle was negligible. Results extracted from the last simulated cycle are presented in the next sections for the coated and uncoated pistons.

Results

In this section the numerical setup is first validated against experimental data for the metallic piston configuration. Afterwards, results obtained for metallic and coated pistons are compared to determine the impact of the coating on engine performance.

Combustion validation

In Fig. 11 in-cylinder pressure traces obtained in experiments and simulations are compared. For the metallic piston engine, it can be noticed that numerical results are in satisfactory agreement with

experimental data. Small differences observed for the in-cylinder pressure during combustion development were considered acceptable and consistent with previous results obtained for the engine under study [23]. The pressure traces for the metallic and coated piston configurations are almost over imposed throughout the engine cycle, with the coated engine showing slightly higher in-cylinder pressure near TDC and after the peak pressure. The maximum difference between pressure traces is, however, limited to about 0.7 bar.

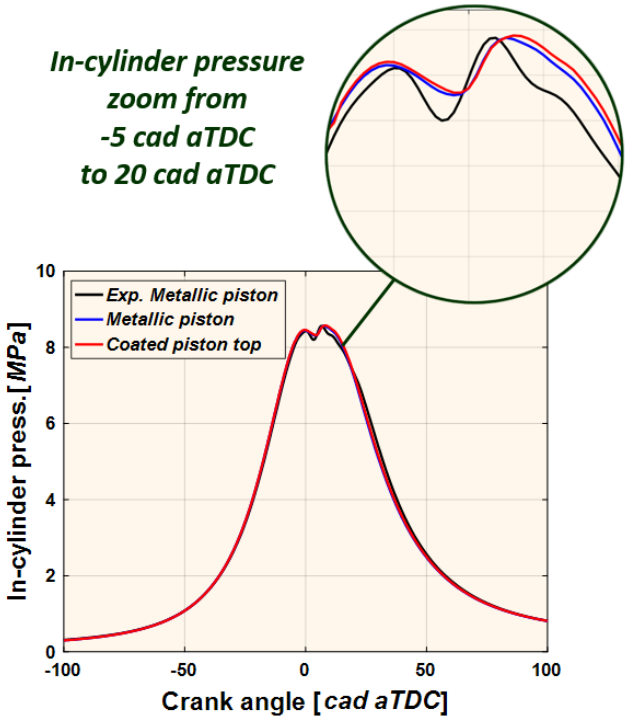

Figure 11. Calculated in-cylinder pressure traces for standard metallic piston and coated piston top cases, compared with experimental data acquired with the metallic piston.

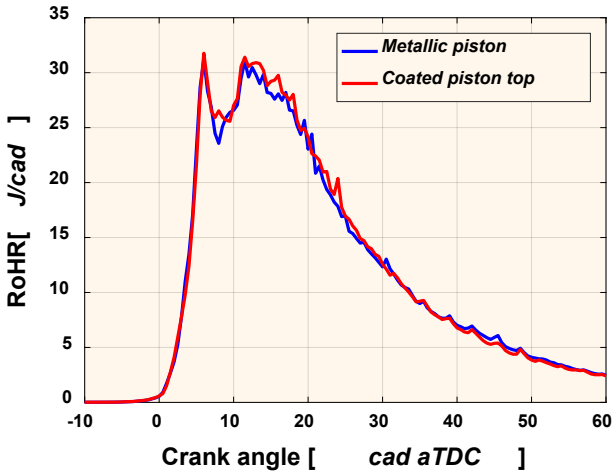

Figure 12. Calculated rate of heat release for standard metallic piston and coated piston top cases for the last simulated cycle.

Fig. 12 shows the rate of heat release (RoHR) of the last simulated cycle of both calculations. The case of the coated piston top shows slightly higher energy release rate during the first part of the combustion, between 0 CAD aTDC and roughly 30 CAD aTDC. Afterwards the rate of heat release becomes lower for the coated piston top, during the expansion stroke. These characteristics highlight that the combustion develops faster for the coated piston top case when compared to the standard metallic piston, possibly a consequence of the lower combustion heat losses during early combustion. This is confirmed by data in Table 3 where characteristic combustion angles are compared for the two configurations studied. The MFB50 (Mass Fraction Burnt 50%) crank angles are almost identical between the metallic and the coated piston configurations; however, the MFB10-90 crank angles show a significantly faster combustion development for the coated piston.

Table 3. Comparison of characteristic combustion angles

Variable	Standard metallic piston	Coated piston top
MFB50 [CAD]	19.2	19.1
MFB10-90 [CAD]	45.1	43.3

CHT wall temperatures

The converged mean temperatures of both configurations piston bowl and piston top are shown in Fig. 13. In the case of the piston bowls, the temperature swings are very similar, as expected since there is no coating on either. However, the temperature of the coated configuration is around 10 K lower than that of the metallic bowl.

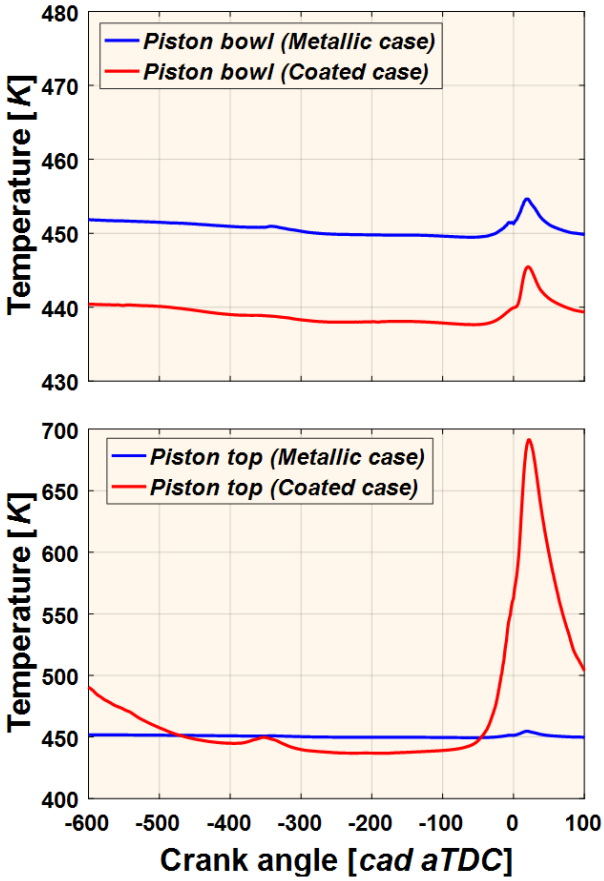

Figure 13. Temporal evolution of the fluid/solid interface temperature for selected piston surfaces: piston bowl (top) and piston top (bottom).

The temperature swing of the coated piston top is significantly higher than that of the metallic configuration, about 265 K according to 3D-CFD-CHT results. Further details concerning the predicted maximum temperature swing are shown in Table 4.

Table 4. Maximum wall temperature swing of piston gas exposed surfaces.

Piston surface	Maximum surface-averaged temperature swing predicted by CHT [K]	
	Standard metallic piston	Coated piston top
Piston bowl	6.1	8.3
Piston top	6.1	264.5

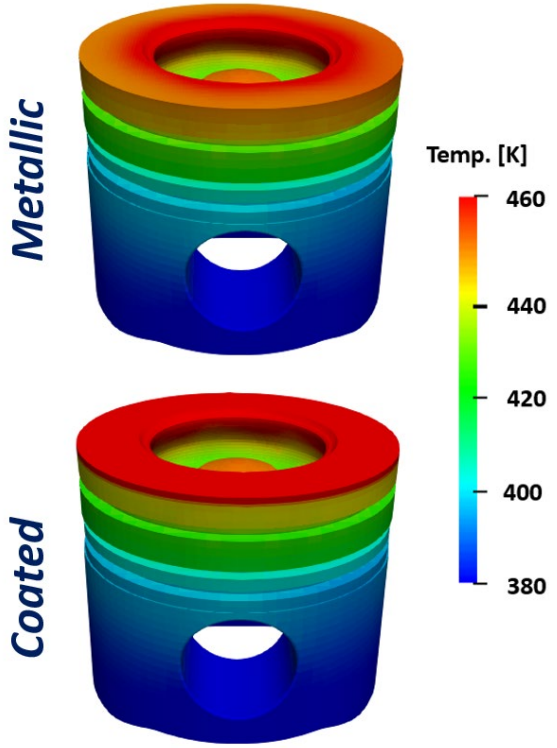

Figure 14. Cycle averaged temperature distribution in the pistons under study: conventional metallic piston (top) and coated piston top (bottom).

To further analyze the effect of the coating layer, the spatial distribution of the cycle-averaged solid piston temperature is shown in Fig. 14 for both configurations. As expected, the highest wall temperatures are reached for the coated engine configuration, and in both cases the temperature rapidly decreases when moving from the surface exposed to combustion gases to the bottom of the piston. The lowest temperatures are observed at the inner cavity and in the piston skirt. Moreover, the temperature gradient is mostly axisymmetric, which is somewhat expected given that a multi-hole Diesel injector was simulated, and axisymmetric boundary conditions were considered on the piston lower surfaces. Small asymmetries on the piston top temperature distributions are caused by the cycle-averaged in-cylinder gases temperature field, which is influenced by the temperature difference between intake and exhaust valves. Furthermore, the spatial temperature distribution calculated on the piston is in good agreement with the results found by other authors [34].

Additional details concerning the piston wall temperatures are shown in Figs. 15 and 16. For both configurations, the hottest area on the piston surface is located at the lip of the bowl, but temperature levels are significantly higher for the coated piston top due to the low heat capacitance of the coating material. Fig. 15 in particular, shows that the piston thermal field is almost time independent for the metallic piston, thanks to the high thermal inertia of the aluminum, while a significative change of piston top temperature can be clearly noticed for the coated piston configuration. The latter is a clear sign of the low thermal inertia of the coating material, which tends to follow closely the gas temperature during the combustion process. At 10 CAD aTDC the coated piston top is already showing local high-temperature spots near the lip of the bowl, caused by the combustion of adjacent gases, which reached a peak in RoHR at +5 CAD aTDC

(Fig. 12). As a result of the described phenomena, the maximum thermal gradient on the metallic piston top surface is about 40 K at 20 CAD, while for the coated piston it is about 330 K at the same instant.

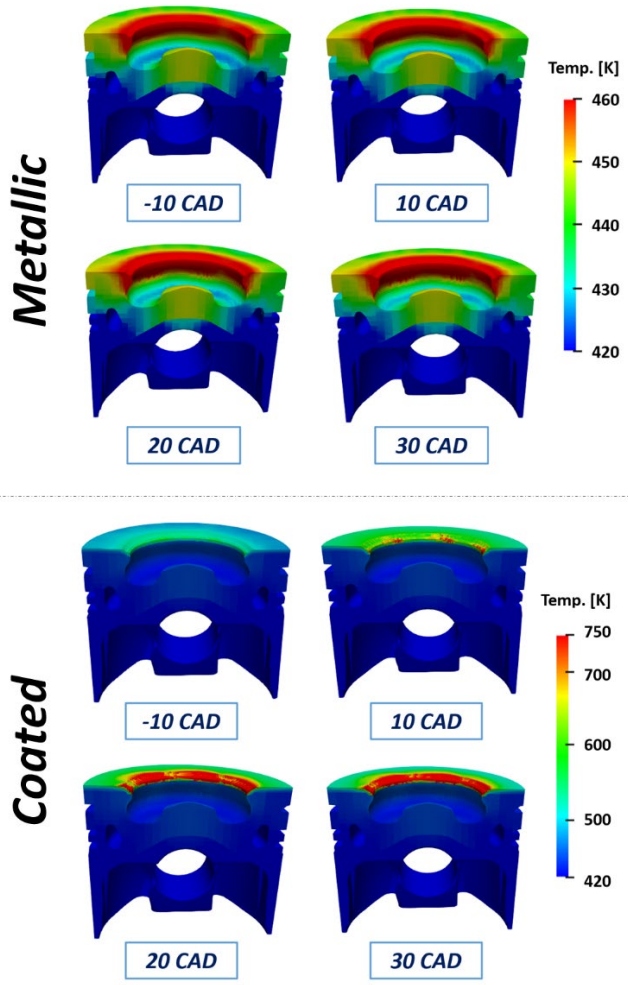

Figure 15. Temperature distribution on piston gas exposed surfaces and interior at selected crank angles: metallic piston (top) and coated piston top (bottom).

Fig. 16 adds further details concerning the heat transfer within the piston for the two studied configurations. Main differences between pistons' thermal fields are mostly limited to the coating layer because the low thermal conductivity of the coating material limits heat transfer towards aluminum. Temperature distribution within the aluminum is therefore similar between the coated and metallic pistons, with a minimum temperature observed at piston skirt surface. Fig. 16 also highlights a significant change in temperature gradient at the interface between the coating layer and the aluminum. This phenomenon is caused by the different thermal conductivities of the two materials, which differ by almost two order of magnitudes.

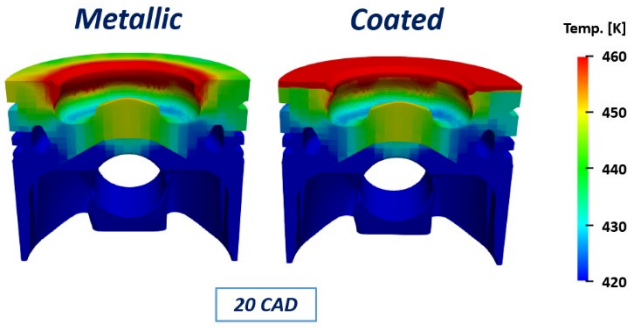

Figure 16. Comparison of temperature distribution between metallic piston (left) and coated piston top (right) at +20 CAD aTDC.

Heat transfer analysis

To analyze the effect of the coating on heat losses, the total heat transfer on each boundary of the combustion chamber was quantified for both engine configurations and presented in Fig. 17. The total heat transferred through all the walls of the combustion chamber is lower for the coated piston configuration (-8.8% compared to the metallic engine). Considering each wall separately, the heat transferred to the piston presents the highest values in both configurations. The largest difference is observed for the piston top (-29.2% in coated piston) due to the temperature swing of the coating layer. It is worth noting that the total heat transfer through the piston represents 60% and 55% of the total heat transfer through the in-cylinder walls in the metallic and coated configurations, respectively. Additionally, the resulting heat balance is in good agreement with literature data reported by other authors for Diesel engines [35]. The details of the differences in heat transfer for both configurations are listed in Table 5.

Table 5. Calculated heat transfer within the combustion chamber.

Combustion chamber wall	Metallic engine [J]	Coated engine [J]	Difference [%]
Piston bowl	27.46	26.50	-3.50
Piston top	26.16	18.53	-29.17
Total piston	***53.62***	***45.03***	***-16.02***
Liner	***19.58***	***20.23***	***3.32***
Head surf.	8.43	8.61	2.14
Int. valves	4.20	4.30	2.38
Exh. valves	3.57	3.63	1.68
Total head	***16.20***	***16.54***	***2.10***
Total engine	**89.41**	**81.80**	**-8.81**

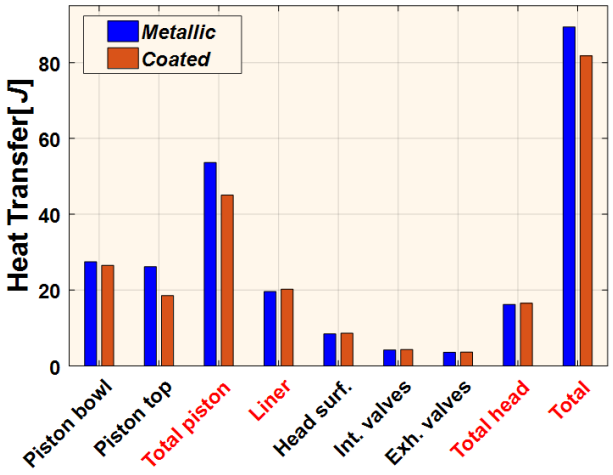

Figure 17. Heat transfer comparison between metallic and coated piston engines.

As in both calculations the liner and cylinder head are assumed isothermal, differences in heat transfer resulting on these boundaries are to be attributed to the effects of heat transfer coefficients and gas temperature only. According to the heat balance shown in Fig. 17 the application of the thermal coating seems to slightly affect the heat transfer through the uncoated combustion chamber walls (liner, head and valves). To explain these differences, the average gas temperature and heat transfer coefficient in two of the uncoated walls (Piston bowl and Liner) are shown in Fig. 18.

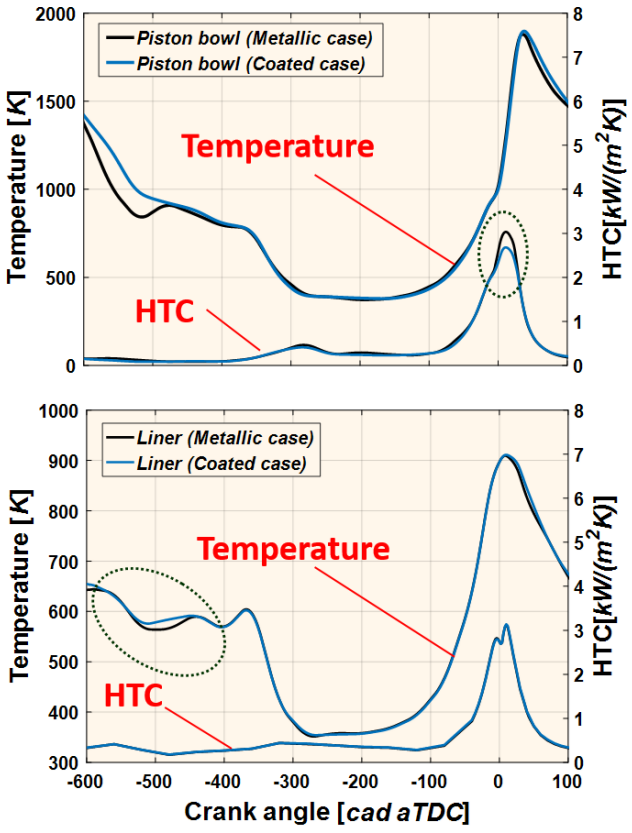

Figure 18. Near wall gas temperature and heat transfer coefficient HTC of piston bowl (top) and liner (bottom) for the metallic piston and coated piston top cases. Highest differences are highlighted with dashed circles.

Concerning the piston bowl, significant differences in HTC between coated and metallic cases are observed during the combustion phase. Indeed, the HTC for the uncoated case is higher than for the coated piston case during early combustion development, while the gas temperature is almost superimposed in the same engine period and starts to diverge after +20 CAD aTDC. The resulting heat losses towards the bowl are therefore higher with the metallic piston; this partially justifies the slower combustion development shown in Fig. 12 and Table 3. The higher HTC observed in the metallic piston configuration is the result of a larger liquid film mass deposited on the surface of the bowl during early combustion development (Fig. 19), an aspect that is known to significantly increase heat transfer. Liquid film dynamics is probably affected by the presence of the temperature swing characterizing the coated piston top and its consequences on gas-wall heat transfer. In particular, during early combustion development the reacting mixture is in close contact mainly with the bowl lip and piston top boundaries. The thermal swing of the coating layer reduces gas heat rejection towards the piston top and favors gas heat transfer towards the bowl and the liquid spray, compared to the metallic piston case. The higher local gas heat rejection in the coated piston case enhances fuel evaporation and reduces liquid film formation on the piston bowl, with the overall effect of reducing the gas-to-bowl heat transfer coefficient around combustion TDC compared to the metallic piston case (Fig. 18). Although the bowl gas temperatures in the coated configuration are higher during the exhaust phase (-700 CAD to – 450 CAD), the role of the HTC is predominant and leads to an overall decrease of cyclic heat losses in the coated piston configuration.

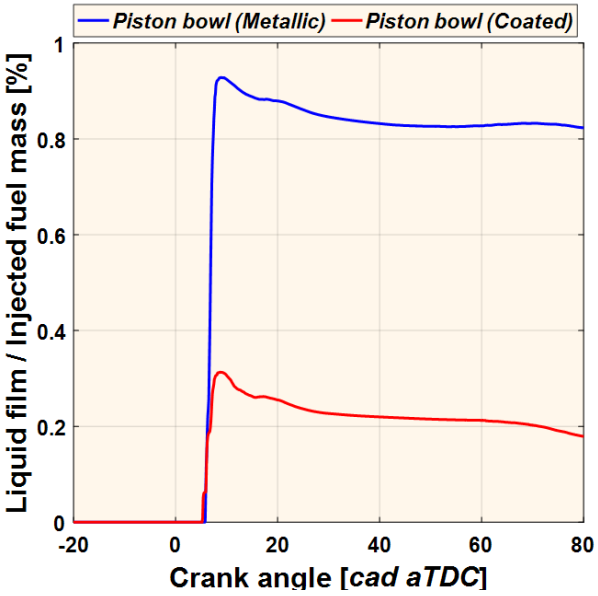

Figure 19. Liquid film mass fractions calculated on bowls surfaces for the metallic piston and the coated piston cases.

In the case of the liner, the HTC traces are almost superimposed throughout the full engine cycle for both piston configurations. However, higher gas temperatures during exhaust and combustion phases are observed with the coated piston and, consequently, the cyclic heat losses through the liner are higher than in the metallic piston configuration (Table 5).

Finally, engine efficiencies are compared in Table 6. The reduction of 8.8% in heat losses results in an improvement of the indicated efficiency of the engine for the coated piston configuration. This

effect seems to be related with the increase in combustion efficiency due to the coating layer.

Table 6. Comparison between metallic and coated piston top engines performance: volumetric, combustion and indicated efficiencies.

Engine efficiency	Metallic engine [%]	Coated engine [%]
Combustion efficiency	98.2	98.9
Indicated efficiency	39.03	39.58

Conclusions

In this paper a study of the heat transfer through metallic and thin coated Diesel engine pistons was carried out. First a novel approach has been proposed and employed to overcome typical numerical limitations concerning the modelling of thin coating layers in 3D-CFD CHT simulations.

The proposed methodology consists in the definition of a thick coating layer reproducing the thermal behavior of the thin coating. To this aim, for a specific thickness of the thick layer, a 1D-HTM based multifactorial DoE was used in combination with a multiple regression analysis to identify the most suitable physical properties of the equivalent coating layer material (thermal capacitance and conductivity).

3D-CFD CHT simulations were then performed to assess engine performance for metallic and coated piston top configurations, and validated against experimental data acquired for the metallic piston engine. Results showed that the combustion development is faster with the coated piston, probably due to the lower heat losses in the first part of the combustion, as confirmed by an analysis of HTC and gas temperature acting on the piston bowl. For the piston top, the temperature swing obtained with the metallic piston is in agreement with literature data, while in the coated configuration the maximum temperature swing is about 265 K. 3D visualization of the piston top thermal field highlighted that the bowl lip is the zone of the piston reaching the highest temperature during the engine cycle, especially in the coated piston configuration due to the lower thermal inertia of the coating material. The local temperature in the coated piston can reach levels as high as 750 K during combustion.

CHT calculations showed that the overall heat transfer between in-cylinder gases and combustion chamber walls is reduced with a smart coating layer on the piston top (-8.81%). Most of the reduction is observed in the piston (-16.02%), while a slight increase of heat transfer between gases, head and liner is observed (+2.1% and +3.32% respectively) with the coated piston configuration. The latter is mainly caused by increased gas temperature during the combustion and exhaust phases of the engine cycle.

Finally, due to the application of a coating layer, the reduction in heat losses leads to improvements of 0.7%, and 0.5% in the combustion and indicated efficiencies, respectively.

Current technological limitations in experimental tests do not allow a validation of 3D-CFD CHT simulations results, which clearly constitutes a limit of the present study. However, it is worth highlighting that numerical simulations are therefore the only available tool that can be used nowadays to investigate coating materials performance in real engine applications with the required level of detail. The crank-angle resolved evolution of the solid components thermal field, as well as the interaction between coating thermal swing and surrounding gases/liquids, as an example, are the kind of information that can be obtained only through 3D-CFD CHT simulations, especially in high-speed medium load engine conditions such as those addressed in the present study.

References

1. Soltani, R., Samadi, H., Garcia, E., and Coyle, T. W., “Development of alternative thermal barrier coatings for diesel engines”, SAE Technical Paper 2005-01-0650, 2005, doi:10.4271/2005-01-0650.
2. Kosaka, H., Wakisaka, Y., Nomura, Y., Hotta, Y., Koike, M., Nakakita, K., and Kawaguchi, A., “Concept of ‘temperature swing heat insulation’ in combustion chamber walls, and appropriate thermo-physical properties for heat insulation coat”. SAE Int. J Eng., 2013, doi:10.4271/2013-01-0274.
3. Kikusato, A., Terahata, K., Jin, K., and Daisho, Y., “A Numerical Simulation Study on Improving the Thermal Efficiency of a Spark Ignited Engine---Part 2: Predicting Instantaneous Combustion Chamber Wall Temperatures, Heat Losses and Knock---“. SAE Int. J. Engines, 2014, doi:10.4271/2014-01-1066.
4. Kogo, T., Hamamura, Y., Nakatani, K., Toda, T., Kawaguchi, A., and Shoji, A., “High Efficiency Diesel Engine with Low Heat Loss Combustion Concept-Toyota’s Inline 4-Cylinder 2.8-Liter ESTEC 1GD-FTV Engine”. SAE Technical Paper, 2016-01-0658, 2016, doi:10.4271/2016-01-0658.
5. Andrie, M., Kokjohn, S., Paliwal, S., Kamo, L. S., Kamo, A., and Procknow, D., “Low heat capacitance thermal barrier coatings for internal combustion engines”, SAE Technical Paper, 2019-01-0228 , 2019, doi: 10.4271/2019-01-0228.
6. Fukui, K., Wakisaka, Y., Nishikawa, K., Hattori, Y., Kosaka, H., and Kawaguchi, A., “Development of instantaneous temperature measurement technique for combustion chamber surface and verification of temperature swing concept”, SAE Technical Paper, 2016-01-0675, 2016, doi: 10.4271/2016-01-0675.
7. Rakopoulos, C. D., and Mavropoulos, G. C., “Study of the steady and transient temperature field and heat flow in the combustion chamber components of a medium speed diesel engine using finite element analyses”, Int. J. Energy Res., 20(5): 437-464, 1996.
8. Rakopoulos, C. D., and Mavropoulos, G. C. (1998). “Components heat transfer studies in a low heat rejection DI diesel engine using a hybrid thermostructural finite element model”, App. Therm. Eng., 18(5): 301-316, 1998, doi: 10.1016/S1359-4311(97)00055-0.
9. Fontanesi, S., and Giacopini, M., “Multiphase CFD–CHT optimization of the cooling jacket and FEM analysis of the engine head of a V6 diesel engine”. App. Therm. Eng., 52(2): 293-303, 2013, doi: 10.1016/j.applthermaleng.2012.12.005.
10. Kundu, P., Scarcelli, R., Som, S., Ickes, A., Wang, Y., Kiedaisch, J., and Rajkumar, M., “Modeling heat loss through pistons and effect of thermal boundary coatings in diesel engine simulations using a conjugate heat transfer model”, SAE Technical Paper, 2016-01-2235, 2016, doi: 10.4271/2016-01-2235.
11. Leguille, M., Ravet, F., Le Moine, J., Pomraning, E., Richards, K., and Senecal, P. K., “Coupled fluid-solid simulation for the prediction of gas-exposed surface temperature distribution in a SI engine”, SAE Technical Paper, 2017-01-0669, 2017, doi: 10.4271/2017-01-0669.

12. Wu, M., Pei, Y., Qin, J., Li, X., Zhou, J., Zhan, Z. S, and Hu, T. G., “Study on methods of coupling numerical simulation of conjugate heat transfer and in-cylinder combustion process in GDI engine”, SAE Technical Paper, 2017-01-0576, 2017, doi: 10.4271/2017-01-0576.
13. Zhang, L., “Parallel simulation of engine in-cylinder processes with conjugate heat transfer modeling”. Appl. Therm. Eng., 142: 232-240, 2018, doi:10.1016/j.applthermaleng.2018.06.084.
14. Hummel, D., Beer, S., and Hornung, A., “A conjugate heat transfer model for unconstrained melting of macroencapsulated phase change materials subjected to external convection”, Int. J. Heat Mass Transfer, 149:119205, 2020, doi:10.1016/j.ijheatmasstransfer.2019.119205.
15. Monelletta, L., “Contribution to the study of combustion noise of automotive Diesel engines”, Doctoral dissertation, Universitat Politècnica de València, 2010.
16. De Lima Moradell, D. A., “Analysis of combustion concepts in a poppet valve two-stroke downsized compression ignition engine designed for passenger car applications”, Doctoral dissertation, Universitat Politècnica de València, 2016.
17. Broatch, A., Margot, X., Garcia-Tiscar, J., and Escalona, J., “Validation and Analysis of Heat Losses Prediction Using Conjugate Heat Transfer Simulation for an Internal Combustion Engine”, SAE Technical Paper, 2019-24-0091, 2019, doi: 10.4271/2019-24-0091.
18. Olmeda, P., Margot, X., Quintero, P., and Escalona, J., “Numerical approach to define a thermodynamically equivalent material for the conjugate heat transfer simulation of very thin coating layers” Int. J. Heat Mass Transfer, 162:120377, 2020 ,doi:10.1016/j.ijheatmasstransfer.2020.120377.
19. Broatch, A., Olmeda, P., Margot, X., and Escalona, J., “New approach to study the heat transfer in internal combustion engines by 3D modelling”, Int. J. Therm. Sci., 138:405-415, 2019, doi: doi.org/10.1016/j.ijthermalsci.2019.01.006.
20. Broatch, A., Olmeda, P., Margot, X., and Escalona, J., “Conjugate Heat Transfer study of the impact of ‘thermo-swing’ coatings on Internal Combustion Engines heat losses”, Int. J. Engine Res., 2020, doi: 10.1177/1468087420960617.
21. Broatch, A., Olmeda, P., Margot, X., and Gomez-Soriano, J., “A one-dimensional modeling study on the effect of advanced insulation coatings on internal combustion engine efficiency”. Int. J. Engine Res., 1468087420921584, 2020, doi: 10.1177/1468087420921584.
22. Senecal, P.K., Richards, K., and Pomraning, E., “CONVERGE 2.4 Manual,” Madison, WI, 2019.
23. Gómez Soriano, J., “Computational assessment of combustion noise of automotive compression-ignited engines”, Doctoral dissertation, Universitat Politècnica de València, 2018.
24. H. K. Versteeg, W. Malalasekera, “An Introduction to Computational Fluid Dynamics – The Finite Volume Method”, 2nd edition, Pearson Educational Limited, 2007.
25. Bredberg, J., “On the wall boundary condition for turbulence models”, Chalmers University of Technology, Department of Thermo and Fluid Dynamics, Internal Report 00/4, Goteborg, 2000.
26. Habchi, C., Lafossas, F. A., Béard, P., and Broseta, D., “Formulation of a one-component fuel lumping model to assess the effects of fuel thermodynamic properties on internal combustion engine mixture preparation and combustion”. SAE transactions, 1421-1431, 2004, doi: 10.4271/2004-01-1996.
27. O'Rourke, P. J., and Amsden, A. A., “A particle numerical model for wall film dynamics in port-injected engines”, SAE transactions, 2000-2013, 1996, doi:10.4271/961961.
28. Senecal, P. K., Pomraning, E., Richards, K. J., Briggs, T. E., Choi, C. Y., McDavid, R. M., and Patterson, M. A., “Multi-dimensional modeling of direct-injection diesel spray liquid length and flame lift-off length using CFD and parallel detailed chemistry”, SAE transactions, 1331-1351, 2003, doi: 10.4271/2003-01-1043.
29. Amsden, A. A., and Findley, M., “KIVA-3V: A block-structured KIVA program for engines with vertical or canted valves”, No. LA-13313-MS Lawrence Livermore National Lab.(LLNL) Livermore, CA (United States), 1997.
30. Broatch, A., Margot, X., Novella, R., and Gómez-Soriano, J., “Impact of the injector design on the combustion noise of gasoline partially premixed combustion in a 2-stroke engine”, Appl. Therm. Eng., 119:530-540, 2017, doi: 10.1016/j.applthermaleng.2017.03.081.
31. Gonera, M., and Sandin, O., “Thermal Analysis of a Diesel Piston and Cylinder Liner using the Inverse Heat Conduction Method”, Goteborg, Sweden, Chalmers University Of Technology, 2015.
32. Lu, Y., Zhang, X., Xiang, P., and Dong, D., “Analysis of thermal temperature fields and thermal stress under steady temperature field of diesel engine piston”, Appl. Thermal Eng., 113:796-812, 2017, doi: 10.1016/j.applthermaleng.2016.11.070 .
33. Paweł, M., Geca, M., "FEM analysis of piston for aircraft two stroke diesel engine", MATEC Web of Conferences, 252:07004, 2019, doi:10.1051/matecconf/201925207004.
34. Esfahanian, V., Javaheri, A., and Ghaffarpour, M, “Thermal analysis of an SI engine piston using different combustion boundary condition treatments”, Appl. Therm. Eng., 26(2-3):277-287, 2006, doi: 10.1016/j.applthermaleng.2005.05.002.
35. Poubeau, A., Vauvy, A., Duffour, F., Zaccardi, J. M., Paola, G. D., and Abramczuk, M. (2019). "Modeling investigation of thermal insulation approaches for low heat rejection Diesel engines using a conjugate heat transfer model", Int. J. Engine Res., 20(1):92-1042019, 2019, doi:10.1177/1468087418818264.

Contact Information

Xandra Margot
CMT-Motores Térmicos. Ed. 6D
Universitat Politècnica de València.
Camino de Vera s/n.
46022 Valencia. Spain.
E-mail: xmargot@mot.upv.es

Andrea Bianco
Powertech Engineering S.r.l.
Via Carolina Invernizio 6.
10127 Torino. Italy.
E-mail: a.bianco@pwt-eng.com

Acknowledgments

The presented work has been conceived as result of a collaboration project between Powertech Engineering and CMT Motores Térmicos within the framework of the doctoral internship program of Universitat Politècnica de Valéncia.

The respondent wants to express its gratitude to CONVERGENT SCIENCE Inc. and Convergent Science GmbH for their kind support for performing the CFD-CHT calculations using CONVERGE software.

Definitions/Abbreviations

1D-HTM	One Dimensional Heat Transfer Model
AMR	Adaptive Mesh Refinement
ARPA-E	Advanced Research Projects Agency - Energy
aTDC	After Top Dead Center
CAD	Crank Angle Degrees
CFL	Courant-Friedrichs-Levy
CHT	Conjugate Heat Transfer
CI	Compression Ignition
3D-CFD	Three Dimensional Computational Fluid Dynamics
DoE	Design of Experiments
EVO	Exhaust Valve Opening
HTC	Heat Transfer Coefficient
HTM	Heat Transfer Model
ICE	Internal Combustion Engine
IVC	Intake Valve Closing
MFB50	Mass Fraction Burnt 50%
MFB10-90	Mass Fraction Burnt 10%-90%
NWT	Near Wall Temperature
RoHR	Rate of Heat Release
SI	Spark Ignition
SiRPA	Silica Reinforce Porous Anodized Aluminum
TBC	Thermal Barrier Coating
TSWIN	Temperature SWing INsulation

Symbols

$[C]$	Capacitance matrix
C_p	Specific heat capacity
Δt	Time interval
e	Original coating layer thickness
h_g	Gas-solid heat transfer coefficient
$[K]$	Conductance matrix
k	Thermal conductivity
L	Metallic substrate thickness
Q	Heat flux
q_+	Positive heat transfer (gas to wall)
q_-	Negative heat transfer (wall to gas)
$q_{+/-}^{error}$	Differences in positive (+) and negative (-) heat transfers between equivalent and real coating layers
ρ	Density
R	Thermal resistance
t	Time
T_g	Gas temperature
$[T^{bc}]$	Boundary conditions temperature vector
$[T^t]$	Temperature vector at time t
$[T^{t+\Delta t}]$	Temperature vector at time $t+\Delta t$
T_w	Wall temperature
x	Spatial coordinate in 1D-HTM model